Proceedings of the ASME 2018 1st International Offshore Wind Technical Conference
IOWTC2018
November 4-7, 2018, San Francisco, CA

IOWTC2018-1061

FATIGUE LIFE ANALYSIS OF OFFSHORE WIND TURBINE SUPPORT STRUCTURES IN AN OFFSHORE WIND FARM

Bryan Nelson
CR Classification Society
Taipei, Taiwan

Yann Quéméner
CR Classification Society
Taipei, Taiwan

ABSTRACT

This study evaluated, by time-domain simulations, the fatigue lives of several jacket support structures for 4 MW wind turbines distributed throughout an offshore wind farm off Taiwan's west coast. An in-house RANS-based wind farm analysis tool, WiFa3D, has been developed to determine the effects of the wind turbine wake behaviour on the flow fields through wind farm clusters. To reduce computational cost, WiFa3D employs actuator disk models to simulate the body forces imposed on the flow field by the target wind turbines, where the actuator disk is defined by the swept region of the rotor in space, and a body force distribution representing the aerodynamic characteristics of the rotor is assigned within this virtual disk. Simulations were performed for a range of environmental conditions, which were then combined with preliminary site survey metocean data to produce a long-term statistical environment. The short-term environmental loads on the wind turbine rotors were calculated by an unsteady blade element momentum (BEM) model of the target 4 MW wind turbines. The fatigue assessment of the jacket support structure was then conducted by applying the Rainflow Counting scheme on the hot spot stresses variations, as read-out from Finite Element results, and by employing appropriate SN curves. The fatigue lives of several wind turbine support structures taken at various locations in the wind farm showed significant variations with the preliminary design condition that assumed a single wind turbine without wake disturbance from other units.

I. INTRODUCTION

In recent years, the Pacific island nation of Taiwan, with its abundant wind energy resources and shallow water depths, has garnered much attention from the international offshore wind energy community. In response, the Taiwanese Ministry of Economic Affairs (MOEA) recently raised its 2025 offshore wind power target to 5.5 GW, with total investment estimated at over US$ 33 billion [1, 2].

One of the more obvious challenges faced by Taiwan's wind farms are the extreme loads exerted on the wind turbine and support structures during typhoons [3, 4], which strike the island, on average, four times every year [5]. Additionally, the authors previously showed that fatigue damage due to Taiwan's prevailing North Easterly trade winds can be just as significant a design problem [6]. This previous study considered the long term environmental loads exerted on the jacket support structure of a single wind turbine during its 20-year design life, and highlighted the sensitivity of the fatigue life to the degree of fluctuation (standard deviation) of the wind loads, as well as the importance of appropriately orienting the jacket foundations according to prevailing wind conditions. This previous study did not, however, consider the exacerbated fatigue loading caused by unsteady wind farm wake effects, such as wake shadowing and wake meandering [7]. These turbine-turbine interactions would certainly be prevalent in the MOEA's "Thousand Wind Turbines" project, which is the motivation behind the design and implementation of the present study.

Section II of this paper describes the target offshore wind farm and target wind turbines, and defines three general regions within the wind farm in terms of the assumed flow conditions at said locations. Section III discusses the short-term ambient environmental conditions, which were stochastically generated in accordance with IEC and DNV guidelines, and the in-farm environmental conditions, for which we employed both analytical and computational models to determine the effects of the upstream wind turbine wakes on the downstream flow field. The numerical models employed to calculate the short-term wind loads on the individual wind farm units and to calculate the flow field throughout the wind farm are respectively described in Sections IV and V, while Section VI briefly presents the hot spot stress evaluation approach which the authors previously showed [6] to produce a good trade-off between computational efficiency and simulation accuracy by combining Finite Element Model (FEM)-derived Closed-Form expressions of the nominal stresses at the tubular joints and stress concentration factors. Finally, the fatigue damage was assessed using the Rainflow Cycle Counting scheme together with appropriate SN curves. The results of the fatigue life assessments for wind turbine support structures at different locations within the wind farm are discussed in the Conclusions.

II. PROBLEM DEFINITION

Phase I of the Formosa I Offshore Wind Farm (Figure 1), located about 3 km off Taiwan's west coast, consists of two Siemens SWT-4.0-120 turbines, which were installed in October, 2016. Phase II, scheduled for 2019, will add another 120 MW, originally planned to be in the form of an additional thirty SWT-4.0-120 turbines. Our study therefore adopted a scaled down version of the 5 MW reference wind turbine proposed by Jonkman et al. [8] at the National Renewable Energy Laboratory. This turbine model was selected due to the availability of the turbine's geometrical and operating specifications, making it a very popular model for benchmark studies, with a wide range of experimental and numerical data available for validation purposes. Our target turbine has a rotor diameter of 120 m, and a rated rotor speed of ω = 12.1 rpm at rated wind speed U = 11.4 m/s.

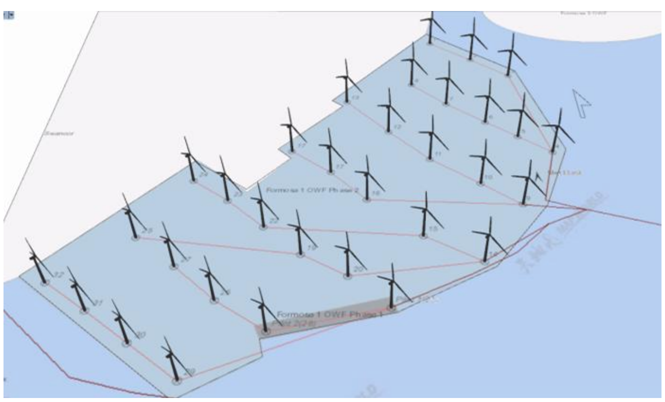

Figure 1. Formosa I Offshore Wind Farm, showing the proposed locations of all 32 Siemens SWT-4.0-120 wind turbines

The rotor geometry is defined in terms of 17 airfoil profiles with specified radial positions, chord lengths, and local twist angles, as summarised in Table 1. The vertex data for each of these airfoils have also been made available, as well as the relationships between wind speed and several operational parameters, such as output power, rotor thrust, rotor speed, blade pitch angle, and so on. Furthermore, Jonkman's included lift and drag coefficients C_L and C_D have been corrected for rotational stall delay using the Selig and Eggars method.

Table 1. NREL 5 MW rotor blade description[8]

Node (-)	RNodes (m)	AeroTwst (°)	DRNodes (m)	Chord (m)	Airfoil Table (-)
1	2.8667	13.308	2.7333	3.542	Cylinder1.dat
2	5.6000	13.308	2.7333	3.854	Cylinder1.dat
3	8.3333	13.308	2.7333	4.167	Cylinder2.dat
4	11.7500	13.308	4.1000	4.557	DU40_A17.dat
5	15.8500	11.480	4.1000	4.652	DU35_A17.dat
6	19.9500	10.162	4.1000	4.458	DU35_A17.dat
7	24.0500	9.011	4.1000	4.249	DU30_A17.dat
8	28.1500	7.795	4.1000	4.007	DU25_A17.dat
9	32.2500	6.544	4.1000	3.748	DU25_A17.dat
10	36.3500	5.361	4.1000	3.502	DU21_A17.dat
11	40.4500	4.188	4.1000	3.256	DU21_A17.dat
12	44.5500	3.125	4.1000	3.010	NACA64_A17.dat
13	48.6500	2.319	4.1000	2.764	NACA64_A17.dat
14	52.7500	1.526	4.1000	2.518	NACA64_A17.dat
15	56.1667	0.863	2.7333	2.313	NACA64_A17.dat
16	58.9000	0.370	2.7333	2.086	NACA64_A17.dat
17	61.6333	0.106	2.7333	1.419	NACA64_A17.dat

Finally, in order to investigate the effects of the exacerbated fatigue loading due to unsteady wind farm wake effects, such as wake shadowing and wake meandering, we focused on wind turbines in three general flow regions of the wind farm, namely along the upstream edge (no wake effects, only ambient wind turbulence considered), at mid-farm (both ambient and single wake turbulence considered, taking into account wind direction and lateral deflection of single wake), and along the downstream edge (highly turbulent coalescence of multiple wakes). The locations of these three flow regions were determined from flow field computations of the entire farm, described in Section V.

III. SHORT-TERM TIME DOMAIN WIND STATES

The concept of wind turbulence is explained in DNV [9] as "the natural variability of the wind speed about the mean wind speed U_{10} in a 10-minute period" for which "the short-term probability distribution for the instantaneous wind speed U can be assumed to be a normal distribution" with standard deviation σ_U. The short-term ambient wind states in the present study were modeled on the IEC 61400-1 Normal Turbulence Model (NTM) [6], with a reference turbulence intensity of I_{ref} = 0.16, in accordance with the requirements of the MOEA [10] that the wind turbines installed in the Formosa I Offshore Wind Farm must be IEC 61400-1 Class I_A compliant. Following the NTM, the standard deviation σ_U of the wind speed for a given U_{10} is calculated by Equation (1):

$$\sigma_U = I_{ref}\,(0.75\,U_{10} + 3.8) \tag{1}$$

To generate more realistic short-term wind states, we employed our previous [6] approach of calibrating the wind speed fluctuations against real on-site data by applying a regression analysis to the wind speed spectra (Figure 2), and then reconstructing the signals (Figure 3, top). The wind speed fluctuations were then randomised (Figure 3, bottom) by randomising the phases of the component harmonics. Finally, the signals were scaled so as to produce a signal which conforms to the IEC's NTM.

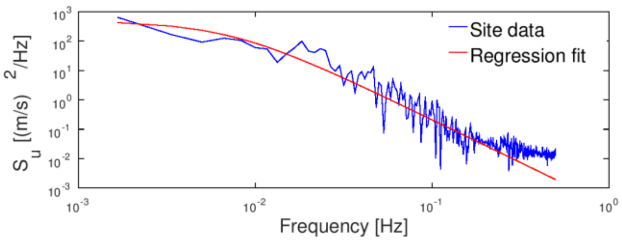

Figure 2. Regression curve fit for PSD of real wind data

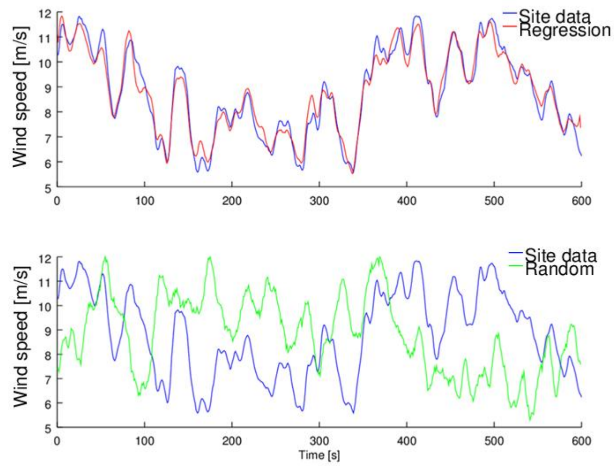

Figure 3. Reconstructed PSDs of real wind data, with corresponding (top) and randomised (bottom) phases

The increased turbulence in the downstream wakes was modelled by means of an analytical model proposed by Larsen [12, 13], which has been shown to reasonably predict the added turbulence I_w in the so-called far wake [14]:

$$I_w = 0.29\, S^{-1/3} \sqrt{1 - \sqrt{1 - C_T}} \tag{2}$$

where S is the distance from the wake-generating upstream wind turbine non-dimensionalised by the rotor diameter D, and C_T is the upstream wind turbine's thrust coefficient. The total turbulence intensity at a downstream turbine is then given by:

$$I_{total} = \sqrt{I_{ref}^2 + \sum I_{w_i}^2} \tag{3}$$

where I_{ref} is the ambient turbulence and I_{w_i} is the wake-added turbulence intensity from the i^{th} upstream wind turbine.

For the mid-farm case, we also considered the effects of wake meander, which is a lateral motion of the wake (Figure 4). To this end, we implemented a Dynamic Wake Meander (DWM) model [15]. In the absence of local data, the stochastic meandering of the wake was derived from wake spectral characteristics obtained from lidar plots in Reference [15].

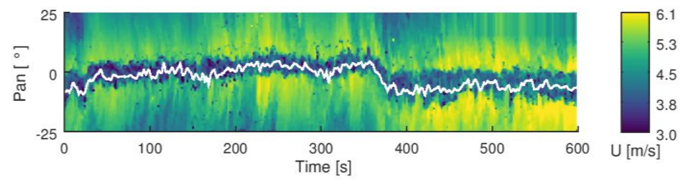

Figure 4. Time history of wake meander behind a single wind turbine (white line shows wake centre-line)

The stochastic lateral motions of the wake were then generated using the same method employed to stochastically generate the short-term wind states, i.e. by applying a regression analysis to the wake centre-line spectra and then reconstructing the signals with randomised phases.

The wake diameter and meander characteristics were then scaled according to the ambient wind speed and the distance from the upstream wind turbine, with scaling factors determined from Wifa3D simulation results. The wake velocity deficit at the target mid-farm wind turbine was modelled as a sinusoidal depression (Figure 5), the centre of which was translated horizontally according to the stochastically generated wake centre-line time series (Figure 6).

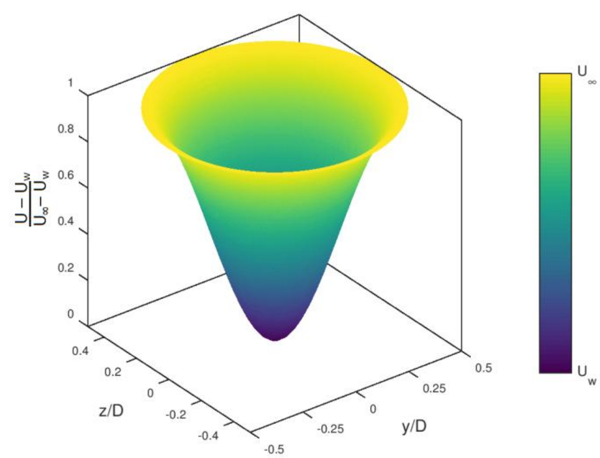

Figure 5. Wake deficit modelled as sinusoidal depression

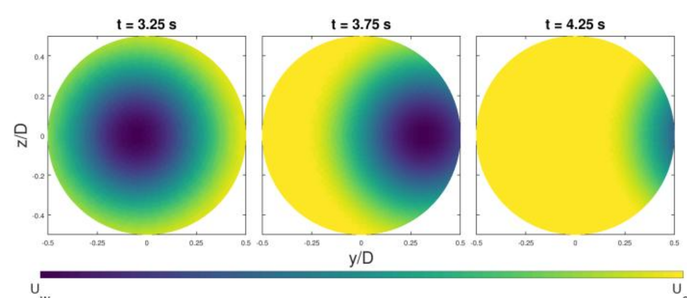

Figure 6. Meander modelled as lateral motion of wake deficit

Finally, we used a Monte Carlo simulation to stochastically generate three months worth of short-term environmental conditions, with the wind speeds and directions based on local wind statistics (Figure 7).

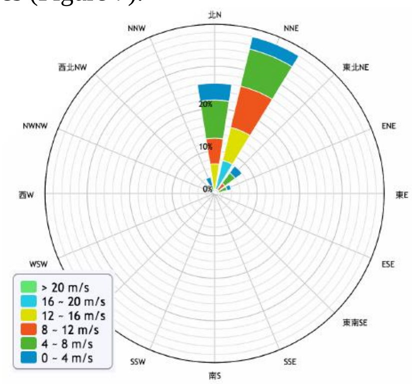

Figure 7. Wind rose off the Chiayi coast [16]

IV. SHORT-TERM TIME DOMAIN WIND LOADS

For the large number of time-domain wind load calculations to be carried out over the simulated life times of the wind turbine support structures, we employed an unsteady blade element momentum method (UBEM). Due to its maturity, the BEM is a very popular tool for the design and analysis of wind turbines [17]. The "blade element" concept discretises the rotor into a number of 2D airfoil sections, such that the total rotor thrust F_N and torque Q may be determined by integrating the airfoil elements' lift C_l and drag C_d characteristics along the length of the rotor blades and multiplying by the number of blades n_B:

$$F_N = n_B \frac{1}{2}\rho U_{rel}^2 \int_0^R (C_l \cos\varphi + C_d \cos\varphi) c \mathrm{d}r$$
$$\mathrm{Q} = n_B \frac{1}{2}\rho U_{rel}^2 \int_0^R (C_l \sin\varphi + C_d \cos\varphi) c r \mathrm{d}r \tag{4}$$

where c is the blade section chord length, U_{rel} is the relative inflow velocity, and φ is the angle of relative inflow.

Our UBEM model includes a wind shear profile, such that for a specified hub height velocity $U(H)$, the wind velocity at height z is given by:

$$U(z) = U(H)\left(\frac{z}{H}\right)^{\alpha} \tag{5}$$

where the power law exponent is taken as α = 0.14, as per DNV recommendation [9] for offshore locations.

Furthermore, a simple, potential flow-based rotor-tower model is also included, which gives the radial and angular components of the flow velocity at a considered point:

$$U_r = U_\infty\left(1 - \frac{R^2}{r^2}\right)\cos\theta$$
$$U_\theta = -U_\infty\left(1 + \frac{R^2}{r^2}\right)\sin\theta \tag{6}$$

and has been validated against a full, unsteady, commercial RANS-solver simulation.

V. WIND FARM FLOW FIELD COMPUTATION

CR recently collaborated with National Taiwan University to develop an in-house, RANS-based wind farm simulation tool, called WiFa3D, which uses a Semi-Implicit Method for Pressure Linked Equations (SIMPLE) algorithm to solve the unsteady, incompressible Reynolds-averaged Navier-Stokes (RANS) equations:

$$\rho\frac{\partial u_i}{\partial x_i} = 0$$
$$\frac{\partial u_i u_j}{\partial x_j} = -\frac{1}{\rho}\frac{\partial p}{\partial x_i} + \frac{\partial}{\partial x_j}\left[\nu\left(\frac{\partial u_i}{\partial x_j} + \frac{\partial u_j}{\partial x_i}\right)\right] - \frac{\partial \overline{u_i' u_j'}}{\partial x_j} \tag{7}$$

with the two-equation k-ε turbulence model (8) to resolve the Reynolds stress, represented by the final term in (7):

$$\frac{\partial}{\partial x_j}(k u_j) = +\frac{\partial}{\partial x_j}\left(\left(\nu + \frac{\nu_t}{\sigma_k}\right)\frac{\partial k}{\partial x_j}\right) + P_k - \varepsilon$$
$$\frac{\partial}{\partial x_j}(\varepsilon u_j) = +\frac{\partial}{\partial x_j}\left(\left(\nu + \frac{\nu_t}{\sigma_\varepsilon}\right)\frac{\partial \varepsilon}{\partial x_j}\right) + c_{\varepsilon 1} P_k \frac{\varepsilon}{k} - c_{\varepsilon 2}\frac{\varepsilon^2}{k} \tag{8}$$

where k is the turbulence kinetic energy, and ϵ is the rate of dissipation of turbulence energy.

The effects of the wind turbines on the flow field through the wind farm are modelled by means of actuator disks, which makes it possible to investigate the flow field throughout a wind farm without the associated computational expense of resolving the Navier-Stokes equations around the individual wind turbine rotors. The so-called actuator disk, like the BEM theory, discretises the rotor into a number of 2D airfoils. The reaction forces of the rotor on the fluid (equal and opposite to the sectional aerodynamic loads on the airfoils, as shown in Figure 8) are calculated by Equation (9), and then imposed on mesoscale RANS [18] or large eddy simulation (LES) [19–21] models of the entire computational domain of a wind farm. The relative inflow velocity for the blade sections are the rotor-coordinate local velocities subtracted from the global ones in the field, as Equation (9) shows.

$$F_n = L\cos\beta - D\sin\beta \quad \text{and} \quad F_t = L\sin\beta - D\cos\beta$$
$$L = \frac{1}{2}\rho|U_{rel}|^2 C_l c dr \quad \text{and} \quad D = \frac{1}{2}\rho|U_{rel}|^2 C_d c dr \tag{9}$$

where
$$U_{rel} = u_{global} - u_{rotor}$$
$$= (u_x + \omega r\sin\psi)\hat{\imath} + (u_y - \omega r\cos\psi)\hat{\jmath} + u_z\hat{k}$$

The WiFa3D code has been validated against experimental and computational data from the Horns Rev Wind Farm [22].

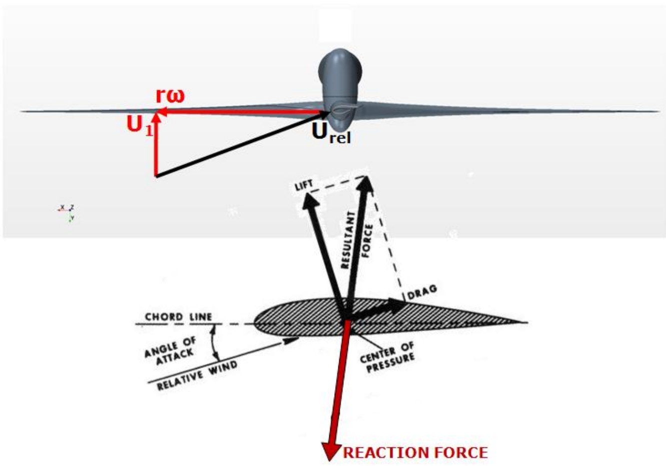

Figure 8. Reaction force on a 2D airfoil element calculated according to local flow field around an operating wind turbine

VI. FATIGUE ASSESSMENT

A structural finite element model of the unit was built using beam elements. It included the tower, the mass of the rotor-nacelle assembly, the jacket, and the four piles, for which the interaction with the soil was reproduced using nonlinear elastic spring connectors. Figure 9 shows the Finite Element Model of the offshore wind turbine's jacket support structure. The computation time required to conduct the static Finite Element Analyses was approximately 0.5 s per time step, which would require several weeks of computations for the millions of wind induced load cycles to simulate during a 20-year design life. To facilitate more rapid fatigue life assessments, a faster approach was adopted which derived from FEA results the Closed-Form (CF) expressions of the nominal stresses at the jacket structure's tubular joint connections as a function of four global load parameters (Figure 9, left), namely:

– the amplitude and direction of the hydrodynamic load (i.e. wave and current on jacket) induced overturning moment at the mudline (OTM_{Hydro} and β_{Hydro}), and
– the amplitude and direction of the wind load (i.e. on the tower and blades) induced overturning moment at the mudline (OTM_{Wind} and β_{Wind}).

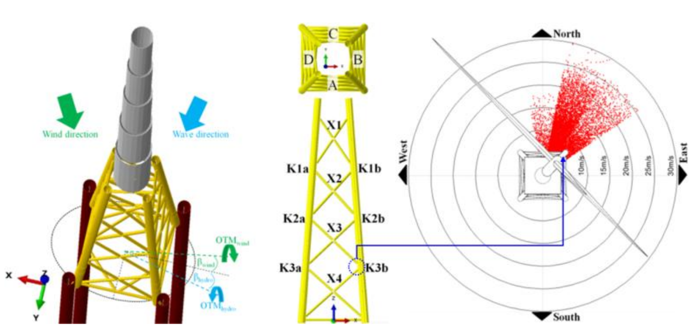

Figure 9. Offshore wind turbine support structure finite element model and CF expressions for load parameters at the mudline

The details of the Closed-Form expression calibration and validation were presented in Reference [6]. Note, however, that in the present study the wave/current load components were omitted to isolate the effects of the wind loads on the fatigue.

This study examined the fatigue life of the highly stressed K-joint 'K3b' (Figure 9, middle) connected to the most exposed legs in view of the predominant NNE wind direction (Figure 9, right). It should be noted that this leg will be mostly undergoing tension stress cycles that will conduct to more critical fatigue damage than at the opposite "downwind" leg which will undergo mainly compression stress cycles [6]. This joint location was deemed sufficiently remote from the tower flange and pile sleeve connections, approximated in the FE model by rigid kinematic couplings, that the nominal stress approach would provide sufficient accuracy for the fatigue analysis at these joints. The hot spot stresses were then calculated at eight spots around the circumference of the intersection of the brace and chord according to DNV GL [22] formulations.

The Closed-Form expression was then employed to convert the wind load fluctuations of each simulated 10-min short-term condition statistically determined into hot spot stresses. The stress range distribution was then obtained by the Rainflow stress cycle counting method, and the fatigue damage was calculated from the 'T' class S-N curve provided by DNV GL [22].

VII. RESULTS

Based on local wind speed and wind direction statistical data (i.e. the wind rose in Figure 7), flow field computations were performed over a range of wind speeds from 6 m/s to 18 m/s for the three predominant wind directions, namely N, NNE, and NE (Figure 10), which together account for 87% of all wind conditions. (Note that the other 13% of wind speeds fall below the target wind turbines' cut-in wind speed.)

From these simulations, we selected three wind turbines which satisfied the three general flow regions described in Section II, namely along the upstream edge (no wake effects, only ambient wind turbulence considered), at mid-farm (both ambient and single wake turbulence considered, taking into account wind direction and lateral deflection of single wake), and along the downstream edge (highly turbulent coalescence of multiple wakes).

The WiFa3D results further served to provide the inlet flow speeds for each of the wake-affected downstream wind turbines for each of the simulated flow conditions. These results were then used to infer the relationship between free stream (ambient) and downstream flow parameters.

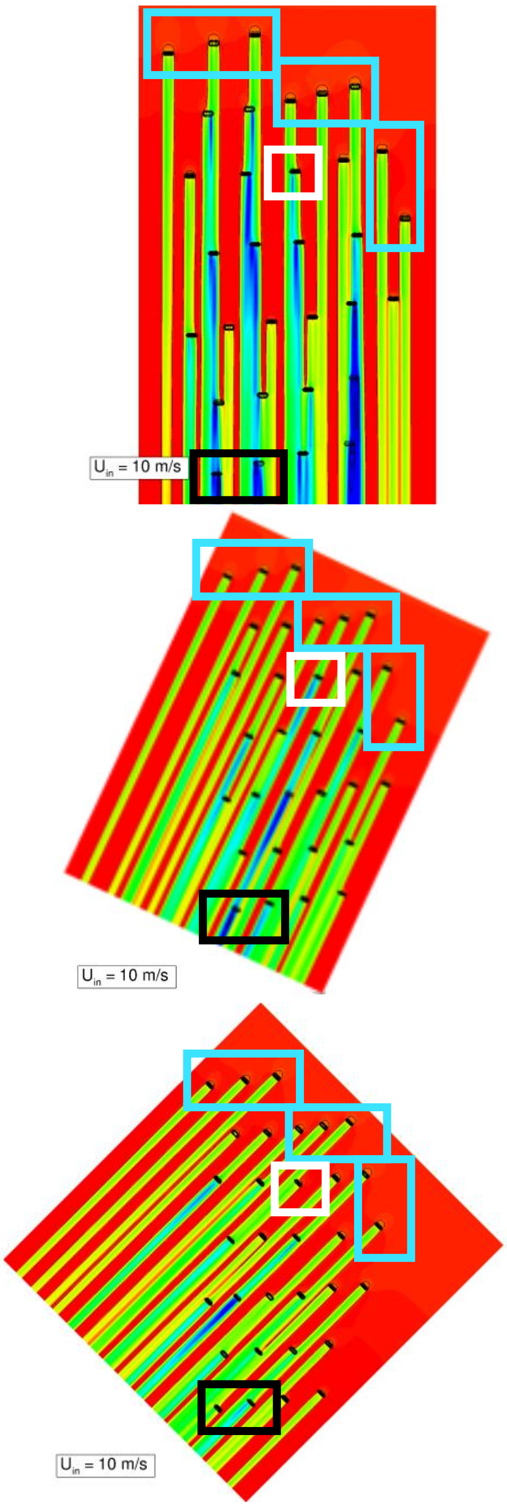

Figure 10. Flow field through target offshore wind farm computed by WiFa3D at three predominant wind directions for U = 10 m/s.

Cyan boxes show wind turbines which satisfy the upstream (undisturbed) flow assumption for all simulated wind directions, the white box shows the mid-farm turbine (single wake) for which wake meander is a critical factor, and the black box show wind turbines which satisfy the downstream (multiple wake) flow assumption.

However, RANS-based actuator disk models have been shown to significantly underpredict the turbulent kinetic energy in the downstream wakes. For this reason, we elected to adopt an empirical model on which to base our downstream wake turbulence calculations. Larsen's model (Equation 2) is very straightforward, requiring as input just the non-dimensionalised distances and the thrust coefficients of the upstream turbines, which were interpolated from the target turbine thrust curve together with the inlet wind speed, again obtained from the WiFa3D simulations, at the upstream wake-generating turbines.

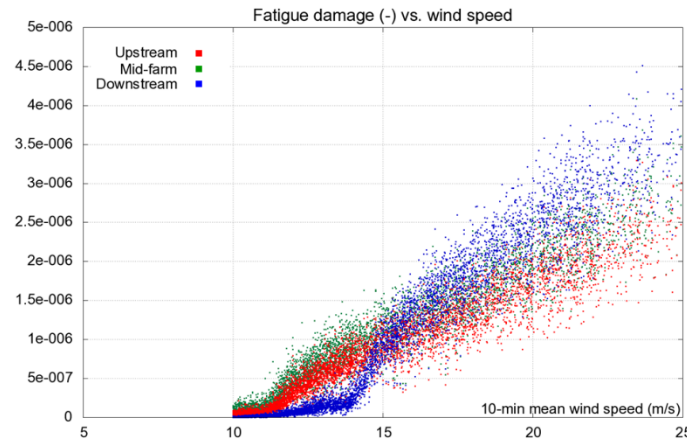

Figure 11. Fatigue damage evaluation for 3 month simulated life time.

Figure 11 shows the fatigue damage inflicted at the considered K-joint's crown toe over a three-month simulated life time (i.e. 13290 × 10-min short-term conditions). It is clear that there is a small jump in the fatigue damage of the upstream turbine (red markers) at ambient wind speeds higher than 11 m/s (recall that the rated wind speed for this turbine is 11.4 m/s). The fatigue damage incurred at the mid-farm wind turbine shows a very similar trend to that of the upstream turbine, except that the mid-farm turbine's incurred damage is slightly higher. On the other hand, the downstream turbine (blue markers) incurs a far more pronounced increase in damage, but only at ambient wind speeds above 14 m/s.

The reason for the significant increase in fatigue damage at mid-farm and downstream may be explained thus:
Reference [6] highlighted the sensitivity of the fatigue life to the degree of fluctuation (standard deviation) of the wind loads. In this paper, we have discussed the wake added turbulence imparted to the flow by the upstream turbines, such that the standard deviation of the wake flow speeds will be higher than that of the ambient flow. At the mid-farm, wind turbines experience even higher fluctuations in flow velocity as the inflow condition alternates between ambient wind and turbulent wake. Therefore, despite the downstream turbines being subjected to lower mean loads, the load fluctuations are larger than those on the upstream turbines, such that the downstream turbines incur more severe fatigue damage.

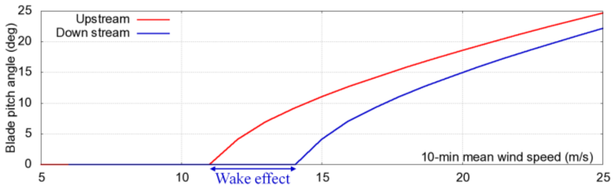

Figure 12. Blade pitch angle control vs. wind speed.

To explain the pronounced increases in fatigue damage at ambient wind speeds of around 12 m/s upstream and at mid-farm, and at around 14 m/s downstream, we present Figure 12, which plots the blade pitch angle against ambient (red) and downstream (blue) wind speeds. This plots shows how the reduction in wind speed due to the wake effects (wake velocity deficit) results in a delay of the blade pitch angle control of about 3 m/s. That is to say that wind turbines along the downstream edge of the wind farm only receive their rated wind speed of 11.4 m/s (the wind speed above which the blade pitch control is activated) at an ambient wind speed of around 14 m/s. As for the sudden increase in fatigue damage at the onset of blade pitch control, this is quite counterintuitive since the purpose of pitching the blade is to reduce aerodynamic loading by reducing the effective angle of attack. However, a secondary consequence of this action is that the blade is now operating in a steeper (more sensitive) region of its lift curve, whereas the load fluctuations on the unpitched blade are, in fact, somewhat relieved by the onset of flow stall. This increased sensitivity to changes in angle of attack combined with exacerbated load fluctuations due to unsteady wind farm wake effects results in a sharp increase in fatigue damage for pitched rotor blades.

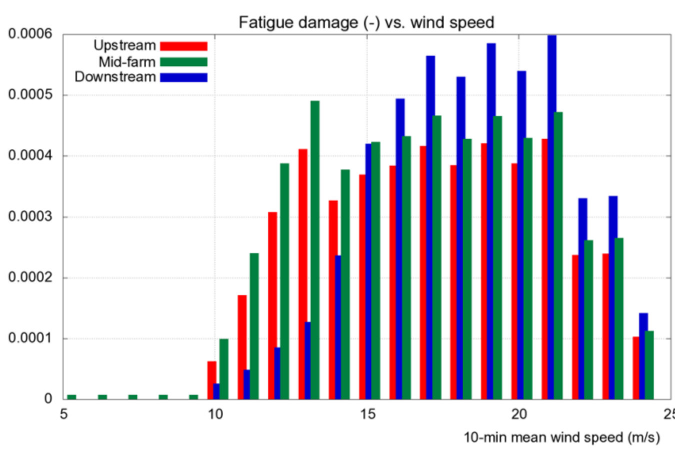

Figure 13. Accumulated fatigue damage distribution for 3 month simulated life time.

Figure 13 shows the accumulated (in 1 m/s bins) fatigue damage distribution, which reiterates how the mid-farm wind turbine shows a similar distribution to the upstream turbine, but with greater incurred fatigue damage. It can also be observed that the distribution of accumulated fatigue of the downstream turbine is the lowest for wind speeds lower than 15 m/s. This is due to the shift of the wind speed at the downstream turbine. Then, for wind speeds above 15 m/s, the distribution of accumulated fatigue damage of the downstream wind turbine is ~30% higher than that of the upstream turbine. This is due to the larger wind fluctuations produced by the wakes of the upwind turbines.

Finally, the total fatigue damages for the three-month simulated life times were 4.55×10^{-3} for the upstream wind turbine, and 5.13×10^{-3} and 4.95×10^{-3} for the mid-farm and downstream turbines respectively, leading to 13% and 9% respective increases in fatigue damage for the mid-farm and downstream wind turbines compared with the upstream ones.

CONCLUSIONS

This study evaluated, by time-domain simulations, the fatigue lives of three jacket support structures for 4 MW wind turbines distributed throughout an offshore wind farm off Taiwan's west coast. Flow field computations were performed for a range of environmental conditions via an in-house RANS-based wind farm analysis tool, WiFa3D, which employs actuator disks to simulate the body forces imposed on the flow field by the target wind turbines. These results were combined with an empirical model to determine the downstream flow parameters.

A long-term statistical environment, based on local offshore wind data, was generated by Monte Carlo simulation, and the short-term environmental loads on the wind turbine rotors were calculated by an unsteady blade element momentum (BEM) model of the target 4 MW wind turbines. Finally, fatigue assessment of the jacket support structures was conducted by applying the Rainflow Counting scheme to the hot spot stresses variations, as read-out from Finite Element results, and by employing appropriate S-N curves.

The exacerbated fatigue loading due to unsteady wind farm wake effects was found to impact the fatigue lives of the downstream turbines, with a 9% increase in fatigue damage over the three-month simulated lifetimes of the far downstream units, and a 13% increase in the fatigue damage of the mid-farm units. Furthermore, these downstream turbines were found to be especially sensitive to load fluctuations around their local rated conditions, where pitch control is activated to, ironically, reduce aerodynamic loading.

REFERENCES

[1] "Taiwan raises 2025 offshore wind target to 5.5GW" https://www.infrastructureinvestor.com/taiwan-raises-2025-offshore-wind-target-to-5-5gw/

[2] "Offshore wind power firms see Taiwan as key to expansion in Asia" https://www.reuters.com/article/us-taiwan-windpower/offshore-wind-power-firms-see-taiwan-as-a-battleground-to-expand-in-asia-idUSKBN1I11IV

[3] T.Y. Lin, Y. Quéméner, "Extreme Typhoon Loads Effect on the Structural Response of Offshore Meteorological Mast and Wind

Turbine", Proceedings of the ASME 2016 35th International Conference on Ocean, Offshore and Arctic Engineering, OMAE2016, 19-24 Jun., 2016, Busan, Korea.
[4] B. Nelson, T.Y. Lin, Y. Quéméner, H.H. Huang, C.Y. Chien, "Extreme Typhoon Loads Effect on the Structural Response of an Offshore Wind Turbine", Proceedings of 7th PAAMES and AMEC2016, 13-14 Oct., 2016, Hong Kong.
[5] FAQ for typhoons. Central Weather Bureau. www.cwb.gov.tw
[6] B. Nelson, Y. Quéméner, T.Y. Lin, H.H.Huang, C.Y. Chien, "Calibration of Long-Term Time-Domain Load Generation for Fatigue Life Assessment of Offshore Wind Turbine", Proceedings of the ASME 2016 36th International Conference on Ocean, Offshore and Arctic Engineering, OMAE2017, 25-30 Jun., June 25-30, 2017, Trondheim, Norway
[7] The Wake Effect: Impacting turbine siting agreements. North American Clean Energy. http://www.nacleanenergy.com/articles/15348/the-wake-effect-impacting-turbine-siting-agreements (21 September 2017)
[8] J. Jonkman, S. Butterfield, W. Musial, and G. Scott., Definition of a 5-MW Reference Wind Turbine for Offshore System Development. Technical Report. NREL/TP-500-38060. February 2009.
[9] DNVGL (2014), Design of Offshore Wind Turbine Structures, DNVGL-OS-J101.
[10] IEC, Wind turbines − Part 1: Design requirements, IEC International Standard 61400-1, 2005.
[11] Ministry of Economic Affair of Taiwan (R.O.C.), "風力發電離岸系統示範獎勵辦法 (Regulations for Demonstration and Rewards of Offshore Wind Power System)", Taiwan, 2012.
[12] G.C.Larsen, J. Højstrup, H.A. Madsen, Wind Fields in Wakes, EUWEC '96, Gothenburg, 1996.
[13] European Wind Turbine Standards II, ECN-C-99-073, 1999
[14] D. J. Renkema, "Validation of wind turbine wake models. Using wind farm data and wind tunnel measurements." MSc Thesis, TU Delft, Netherlands, 2007
[15] Larsen, G. C., Madsen, H. A., Bing¨ol, F., Mann, J., Ott, S., Sørensen, J. N., Okulov, V., Troldborg, N., Nielsen, M., Thomsen, K., Larsen, T. J., and Mikkelsen, R., "Dynamic Wake Meandering Modeling," Tech. Rep. R-1607(EN), Risø National Laboratory, Technical University of Denmark, Roskilde, Denmark, 2007.
[16] 工業技術研究院綠能與環境研究所 http://www.twtpo.org.tw/professional/wind.aspx?kind=Sea
[17] M. Hansen, Aerodynamics of Wind Turbines, 2nd Ed., Earthscan, London, UK, 2007.
[18] Sørensen, J.N.; Shen, W.Z., Numerical modeling of Wind Turbine Wakes. J Fluids Eng 2002, 124, 393–399
[19] Troldborg, N. Actuator Line Modeling of Wind Turbine Wakes. Ph.D. Thesis, Technical University of Denmark, Lyngby, Denmark, 2008.
[20] Troldborg, N.; Sørensen, J.N.; Mikkelsen, R. Numerical Simulations of Wake Characteristics of a Wind Turbine in Uniform Flow Wind Energy 2010, 13, 86–99.
[21] Lu, H., Porté-Agel, F., "Large-Eddy Simulation of a Very Large Wind Farm in a Stable Atmospheric Boundary Layer," Phys Fluids, 2011, 23, 065101
[22] K-C Lee, "A wake model for Wind Turbine Power Prediction", MSc Thesis, National Taiwan University, 2018
[23] DNVGL (2016), Fatigue design of offshore steel structures, DNVGL-RP-C203